Iranian Polymer Journal
https://doi.org/10.1007/s13726-025-01540-9

ORIGINAL RESEARCH

Effectiveness of graphene-polymer nanocomposites on thermo-mechanical and cytotoxicity behavior for dental fillings applications

Abbas Kadhim Hassan[1,2] · Habib Hamidinezhad[1] · Ehssan Al-Bermany[3]

Received: 2 November 2024 / Accepted: 22 June 2025

Abstract

Graphene nano-sheets are one of the most recent and exciting subjects used to reinforce dental filling and various industrial applications. Poly-(methyl methacrylate) (PMMA) and synthesized graphene oxide (GO) were used to restore two types of dental fillings to fabricate dental filler nanocomposites using modified acoustic and sonication procedures. Morphology, structure, thermal, and ultrasound mechanical behavior, as well as cytotoxicity activity, were investigated. X-Ray diffraction (XRD) and Fourier-transform infrared (FTIR) showed a significant change in diffraction behavior and a strong interaction at the interface after adding PMMA and GO nano-sheets for dental fillings. Scanning electron microscopy (SEM) images demonstrated a considerable improvement in homogeneity after the contribution of PMMA within the excellent dispersion of GO in the dental matrix. GO's contribution revealed a critical enhancement in thermal stability of up to 65% using thermogravimetric analysis (TGA). Differential scanning calorimetry (DSC) also showed increase in glass transition temperature (T_g) after the restoration of dental fillings with PMMA and GO nano-sheets. After PMMA and GO nanomaterials contributed, ultrasonic mechanical velocity, compressibility, and elasticity modulus revealed enhanced values up to 50%, 75%, and 160%, respectively. The cytotoxic effect of calcium oxide (X-SUBSTANCES) against rat embryonic fibroblasts (REF) cells was up to 94.92% of the cell viability for restoration nanocomposite fillings. The findings notably improved the thermo-mechanical stability of promisingly developed longer-life dental fillings.

✉ Habib Hamidinezhad
h.hamidinezhad@umz.ac.ir

✉ Ehssan Al-Bermany
ehssan@uobabylon.edu.iq

[1] Department of Physics, Faculty of Basic Sciences, University of Mazandaran, Babolsar 48175-866, Iran

[2] Educational Directorate of Babylon, Ministry of Education, Baghdad 10069, Iraq

[3] Department of Physics, College of Education for Pure Sciences, University of Babylon, Babil 51002, Iraq

Published online: 06 August 2025

Graphical Abstract

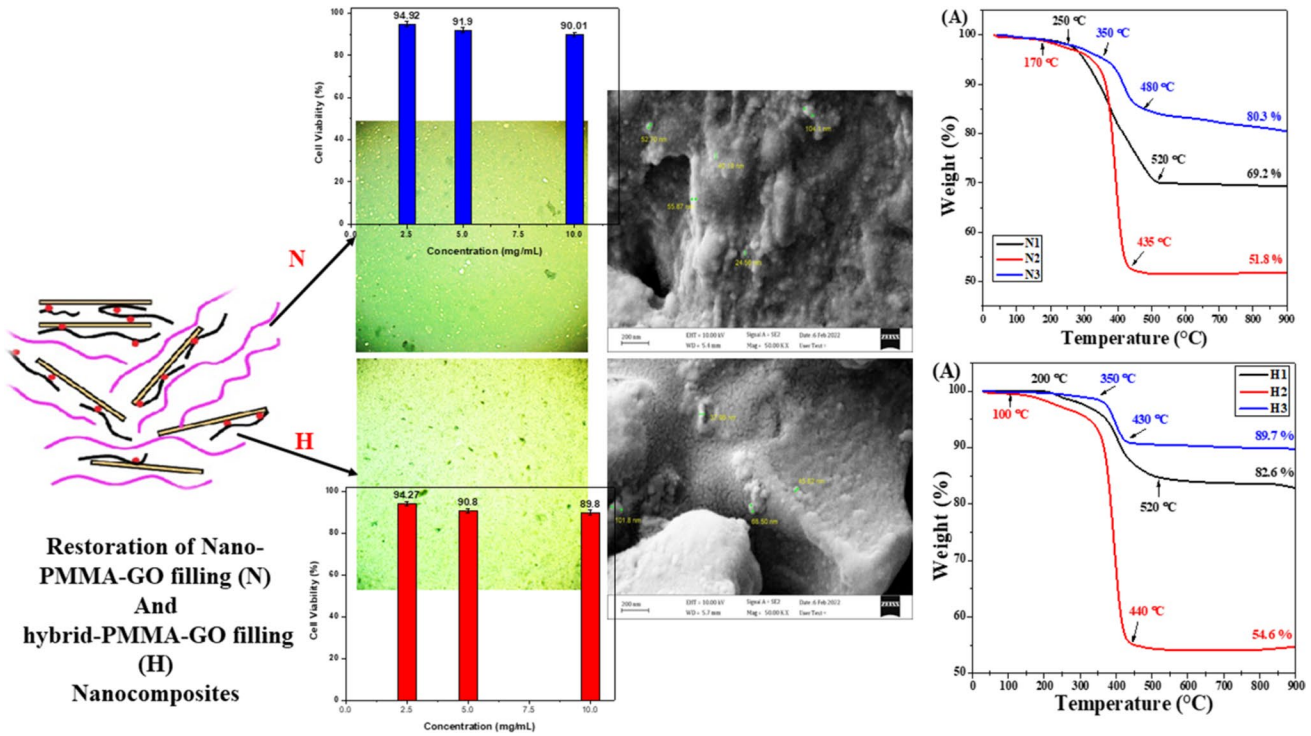

Keywords Cytotoxicity · GO · Dental fillings · PMMA · Restoration · Thermal

Introduction

Resin-based composites are the most popular material in dental restorations because of their superior esthetic quality, mechanical properties, etc. [1]. Moreover, the additives, such as polymers or nanomaterials, utilized in restorative dentistry could adhere to the hard tissues of the teeth, allowing for a non-invasive caries removal technique [2]. Dental resin composite materials have been extensively used as a substitute for dental amalgam materials due to their cosmetic characteristics [3]. Dental resin composites possess superior physical, mechanical, chemical, optical, thermal, and tribological (wear) characteristics compared to older materials filled with amalgam [4]. Composite materials provide superior characteristics compared to conventional polymer matrices [5]. Dental restorative composite materials consist mostly of organic resin matrix and ceramic fillers, which are inorganic [6]. Three primary constituents of the resin matrix are monomers, diluents, photo-initiators, accelerators, and coupling agents [7]. The hybrid-filling technique is commonly used for tooth restorative composite materials. Recently, nanoparticles and nanofibers have become commonly used as innovative fillers because of their exceptional esthetic, bioactivity, and biocompatibility characteristics [8]. Despite these benefits, polymeric composites have significant disadvantages, such as polymerization contraction with affinity for bacterial adhesion [9, 10]. In addition, microorganisms have an easy access to the regenerated dental filling through micro-cavities at the tooth-restoration interface, which exists between the dental restoration and healthy tissues [11].

Many bacteria are responsible for diseases, including ulcers, tooth decay, and gingivitis. Bacteria in the mouth and growing in cavities could produce acid, eroding the tooth's cementum, dentin, and enamel [12]. The decay of teeth is a result of this process when food particles or sugars remain on a tooth's surface, bacteria produce acid [13]. The primary cause of failure is caries at the margin of composite dental restorations [14]. In the last decades, dental fillings have been widely used for anterior and posterior restorations [15]. Unfortunately, research indicates that secondary caries contributes significantly to high failure rate. According to research [16], resin composites build up faster on resin composites than enamel or traditional restorations. Therefore, modifications incorporating antibacterial properties are necessary to expand the service life of resin composite restorations [17]. In addition, composite dental filling materials have endured a series of qualitative and revolutionary

advancements from their first development to the present [18]. Due to the compound's complexity, these materials covered its composition and required properties. In addition, it cannot cause damage to the body, decompose, or release any toxic chemicals while in the mouth [19]. Moreover, this filling must meet various optical standards to show an appropriate view with natural teeth [20]. Thus, clinical, industrial, and research interests in developing, restoring, and anti-biofilm adhesives have increased in recent years using polymers, nanomaterials, or other materials [21].

Polymer is an essential primer or additive material for dentistry [22]. It utilizes various impossible medical applications with alternative materials [23]. Polymers are commonly used for dental bases, provisional crowns, artificial teeth, pigments, cement, endodontics, and tissue conditioners, among other applications [24]. Polymers commonly used in dentistry are polymethyl methacrylate, polyethylene, polyethylene glycol, polycarbonate, polydimethylsiloxane, polyurethane (PUR), polylactic acid, poly(ε-caprolactone), *N*-isopropylacrylamide, *N*-tert-butyl acrylamide, polypyrrole, hexamethyldisilazane, etc. [25]. A denture material must withstand the masticatory burden over an extended period with minimal irritation. The additive material for restoration of the filling must be suitable and not react with the mouth's aqueous environment. It must be without cracking to prevent solvents found in foods, drinks, and medications from entering the filling. The polymer must lack sensitivity to atmospheric conditions in the mouth. It is an outstanding candidate because of its exceptional polymer properties, which include resistance to different conditions, optical, mechanical, thermal, and electrical capabilities, and formability [26]. Poly-(methyl methacrylate) (PMMA), an esteemed candidate for dental polymers, has been in consideration since 1937 [27]. Recently, it has become increasingly well-liked [28], and the most recent research [29]. PMMA ranks it among the top materials for dental fillings [30]. It is cost-effective, simple to manufacture, and possesses advantageous mechanical, physical, and biological characteristics [31]. Additionally, it is applicable in dentistry and is manufactured into long-term repair materials, prosthetic resin, and bone cement, among other products [32, 33].

To resolve problems associated with polymers, lately, dental restorations have incorporated nano-fillers as components [34]. Recent dental applications include graphene oxide (GO) [35], one of the most intriguing nanomaterials. Due to its exceptional qualities and wide range of applications, graphene has piqued scientists' interest [36]. Graphene and its derivative nanomaterials gain increasing popularity in the field of dentistry [37]. It is possible to assess the biocompatibility of these nanomaterials [38]. Graphene-based materials can be adapted to novel applications by modifying their chemical and physical properties [39]. Some things that make graphene unique and exciting are its many functional groups, nano-sized sheets, ability to conduct electricity very well, and mechanical and optical properties [40, 41]. The scientific literature indicates that GO has potent antibacterial properties [42] and other biological and medical applications [43].

This study's objective is to investigate the effect of PMMA and PMMA–GO on the optical properties and antibacterial activity of two dental fillings containing micro- and nano-scale materials. Various characterizations were used to characterize the samples, for instance, FTIR, OPM images, SEM, UV–visible spectroscopy, antibacterial activities, and the effectiveness of the most recent hybrid/nano-dental filling-PMMA/graphene oxide nanocomposites.

Experimental section

Materials

The materials used are listed in Table 1.

Table 1 Summarizes the materials used to prepare samples

Materials	Details	Components	Supplied Company	Country
Beautifil II (H1 sample)	Hybrid filling (Macro and micro-particles)	Bisphenol A-glycidyl methacrylate (1 to 10%), trimethylene glycol dimethacrylate (1 to 5%), Al2O3 (1 to 5%), Aluminofluoro-borosilicate glass (60 to 70%), and DL-camphor quinone (Bis-GMA)	Shofu Inc	Japan
Enhance (N1 sample)	Nano-hybrid universal	Silica nanoparticles (10 to 50 nm), Barium glass, pre-polymer, and Bis-GMA	Sincera Technology	China
PMMA	M_W: 18,000–20000 g/mol	213 ºC: melting point, and 99%: purity	Tuttlingen	China
DMF (Dimethylformamide)	M_W: 73.09 g/mol	99%: purity	Thomas Baker (MIDC)	India
GO	pH of around 5.2	Lap synthesized using the procedure in our previous publication [56], which included complete characterizations	Applying modified Hummer methods [78]	

Fabrication of samples

Table 2 and Fig. 1 reveal the sample preparation scheme in three stages.

Stage 1: Dissolving the raw materials in the solvent.

First, to fabricate H1 and N1 samples, the commercial hybrid and nano-fillings were dissolved in dimethylformamide (DMF) independently using a magnetic stirrer for 6 h to fabricate hybrid-filling named (H1) and nano-fillings named (N1) at room temperature (25 ± 3 °C). The first sample in each group is H1 and N1, which were the reference fillings for comparison with the restoring fillings.

Second, to fabricate H2 and N2 samples, PMMA was dissolved in DMF independently using a magnetic stirrer at room temperature for 2 h. Dissolved PMMA was mixed first with the dissolved H1 to fabricate H2 separately. Also, it was mixed with N1 separately to fabricate N2 dental filling samples. This mixing procedure was continuous for 6 h using magnetic stirring at room temperature (25 ± 3 °C). All the procedures for the samples were carried out separately.

Third, to fabricate H3 and N3 samples, GO was dispersed in DMF for 7 days and sonicated for 30 min daily for complete dispersion at room temperature (25 ± 3 °C). The dispersed GO-DMF was loaded into the restoration hybrid-PMMA dental filling (H2) and mixed for 6 h using a magnetic stirrer at room temperature (25 ± 3 °C). During mixing, the samples were sonicated for 30 min for complete dispersion of the nanomaterials in the matrix of the hybrid-PMMA/GO dental filling (H3). The same procedure was applied to the fabricated nano-PMMA/GO dental filling (N3).

Stage 2: Centrifuge, washing, and casting procedure.

First, the samples were centrifuged to remove DMF, then washed with distilled water, and centrifuged several times to ensure the removal of residual DMF. Some of the samples were left as a solution for specific characterizations, and others were cast in a Petri dish and left in the air at room temperature (25 ± 3 °C) for 4 days until thoroughly dried.

Stage 3: Cytotoxicity test.

A cytotoxicity test was performed for all the samples to ensure they were healthy and not toxic. This is discussed in detail in the "Cytotoxicity test" section.

Table 2 Summarize the sample code and mixing ratio of the components of the restoration samples

Used filling: sample code	Component's concentration (wt. %)		
	Filling	PMMA	GO
Nano Filling: N1	100	00	00
Nano Filling: N2	75	25	00
Nano Filling: N3	75	24	1.0
Hybrid Filling: H1	100	00	00
Hybrid Filling: H2	75	25	00
Hybrid Filling: H3	75	24	1.0

Characterization

The FTIR spectra were measured using a Fourier-transform infrared model Vertex 70 in the wavenumber range

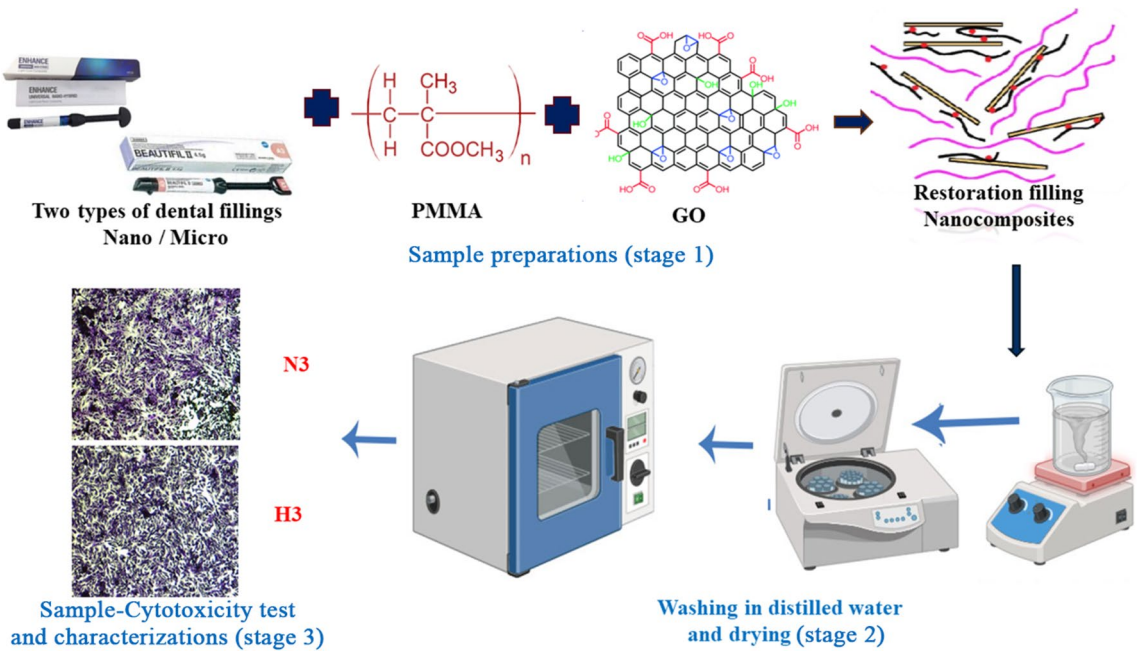

Fig. 1 Scheme explains the steps of sample preparation

4000–500 cm^{-1}, manufactured by Bruker Company, which was made in Germany. 10 runs for each sample as films were utilized to characterize this device and analyze the structure, interactions, functional groups, and any other changes in structure.

The X-ray diffraction instrument (Xpert) utilized the structure between 5 and 90 degrees; both Tescan, made in France, manufactured these devices, and it was used to analyze and measure the structure of materials. The samples were run 28 times for 30 min, and the results were combined automatically by the device.

The surface morphology of the samples was captured using a scanning electron microscope (SEM), manufactured by ZEISS, a German company, with a set of Mag. 50 KX, single A = SE2, 5.4–5.9 nm at 10 kV, resolution 1.0 nm at 15 kV. Meanwhile, Nikon 73,346 optical microscopy (OM), conducted by Olympus Company in Japan, recorded the optical microscopy images with 100X magnification (optical microscopy images in Fig. 1). They were also a film sample, which is considered a great way to obtain information about a sample's surface topography and composition in industries. Several images were recorded for several places in the surface with different magnification SEM and OM microscopy for each sample.

The TGA/DSC instrument, model SDT Q600, manufactured by TA Instruments in the United States, examined thermal behavior between 25 and 900 °C. A sample piece with 2 mg of as films was carried out during the test. It is an important piece of equipment for measuring how the physical properties of a sample change, as well as thermal stability and temperature over time under different air or gas conditions, to test the applicability of dental filling under different conditions and atmospheres.

SV-DH-7A/SVX-7 m, a multi-frequency ultrasound, was utilized at 40 kHz at a fixed frequency for all samples made by the HZDH Company, South Korea. All these devices used films to characterize the samples. The sample was retested 10 times for reliability and to reduce error percentage.

Characterizations used for the cytotoxicity test are a CO_2 incubator and micropipette produced by Cypress Diagnostics from Belgium, a micro-titer reader supplied by Gennex Lab, cell culture plates produced by Santa Cruz Biotechnology from the USA, and a laminar flow hood provided by K & K Scientific Supplier from Korea. This sample was characterized as a solution and discussed briefly in the "Cytotoxicity test" section and Supplementary Material.

Cytotoxicity test

Materials used in the cytotoxicity test

Chemicals and reagents applied are RPMI 1640, fetal bovine serum, and trypsin/EDTA, produced by Capricorn Company, Germany. In contrast, MTT stain is made by Bio-World, and dimethylsulfoxide (DMSO) is provided by Santa Cruz Biotechnology, USA.

Maintenance of cell cultures

Regular cell line REF was upheld in RPMI 1640, then maintained with (10%) of fetal bovine serum in addition to penicillin (100 units/mL) and streptomycin (100 µg/mL). To pass the cells, Trypsin–EDTA was utilized, and then at 80%, it was re-seeded with confluence twice a week. Finally, at 37 °C, it was incubated [44].

Cytotoxicity assays

The MTT assay was utilized on 96-well plates to consider the cytotoxic effect of calcium oxide (X-SUBSTANCES), where the cell lines were planted at × 1*104 cells/well. After 24 h, it was treated with X-SUBSTANCES at various concentrations. Then, after 72 h of treatment, the medium was removed, 100 µL of a 2 mg/mL solution of MTT was added, and the cells were incubated for 2.5 h at 37 °C [44]. Following this, the MTT solution was removed. The remaining crystals in the wells were solubilized using 100 µL of dimethyl sulfoxide (DMSO) and then incubated with shaking at 37 °C for 15 min [45].

A microplate reader was utilized to record the absorbance at 492 nm, whereas the assay is in triplicate. Equation 1 was applied to calculate the cytotoxicity percentage (cell growth inhibition rate)[46]. (1)

$$\text{Cytotoxicity}\ (\%) = \left(A - \frac{A}{B}\right) \times 100 \quad (1)$$

A and *B* mean the optical densities of the control and the test, respectively. At 37 °C and 24 h of incubation with a (1×10^5 cells mL^{-1}) density, the cells were seeded into (24-well micro-titration) plates to visualize the cells' shape using an inverted microscope. It was exposed to X-SUBSTANCES for 24 h, then at 37 °C for 10 to 15 min; the plates were stained, and the crystal violet stain was then incubated [46]. Tap water was utilized to wash off the stain gently until the dye was removed [47]. At (100X) optical magnification, the digital camera was utilized to record the images. The concentration of the sample was 100% (10 mg/mL).

Statistical analysis

The data from three independent experiments were represented as mean ± standard deviation. An unpaired t test was applied to statistically obtain and analyze the data within

the GraphPad Prism 6 to carry out the statistical analysis through the one-way ANOVA analysis of variance. p values less than 0.05 were considered significant, $*p < 0.05$, $p < 0.01$, $*p < 0.001$, and $****p < 0.0001$ [48].

For more or full details of the cytotoxicity test, see Supplementary Material.

Ultrasound mechanical calculations

The relation between the mass of a solution and its volume is defined as density (ρ) and given in Eq. 2 [49]. (2)

$$\rho = \frac{mass\ (m)}{volume(V)} \qquad (2)$$

The density of hybrid dental fillings was higher than that of nano-dental fillings, which increased with the loading of both PMMA and GO in both dental fillings as presented in Table 3. The ultrasound mechanical velocity (V) at 40 Hz frequency was considered using Eq. 3 [50]. (3)

$$V = \frac{x}{t} \qquad (3)$$

(x) thickness and (t) the wave recording time throughout the sample.

The results of both groups of samples presented a notable reduction in compressibility (B), which was calculated using the Laplace equation (Eq. 4) [51]. (4)

$$B = \frac{1}{\rho V^2} \qquad (4)$$

The compressibility finding was significantly improved by redacting the results up to 75% of Ns and 49.5% of Hs samples. In addition, the elasticity modulus (k) improved up to 160% and 75%, respectively, measured using Eq. 5. (5)

$$K = B^{-1} = \rho V^2 \qquad (5)$$

Results and discussion

The FTIR spectra of Hs and Ns samples presented in Fig. 2 range from 500 to 4000 cm^{-1}. In Fig. 2a, H1 revealed the abroad peak of O–H groups at 3491 cm^{-1}, C–H_2 at 2934 cm^{-1}, C=O at 1718 cm^{-1}, C–H at 1456 and 1161 cm^{-1}, C–O at 930 cm^{-1}, and C=C at 684 cm^{-1}. H2 presented the same peaks of H1 with small shifting in O–H and C–H groups as in Fig. 2a, and the C=C peaks presented clearly at 1640 with 1160 cm^{-1} of C–H. H3 presented the main change in the wavenumber area between 1700 and 600 cm^{-1}. It showed big changes by shifting the functional groups like O–H, C–H, and C–O from 3491 to 3367 cm^{-1} and 2937 to 2955 cm^{-1}, as well as stronger peaks at 1456 and 1157 cm^{-1} and other peaks less than 1000 cm^{-1} compared to H1 and H2 [52].

In contrast to the Hs group, the Ns group displayed distinct behavior. Specifically, in Fig. 2b, the nano-denial filling N1 demonstrated three prominent peaks: C=O at 1718 cm^{-1}, C-Hat 1438 cm^{-1}, and C–O at 1052 cm^{-1}. The loading of PMMA in the nano-fillers in N2 revealed the sign of PMMA at C–H at 2947 cm^{-1}, and C=C at 972 cm^{-1} in addition to an increase in the intensity of C=O at 1718 cm^{-1}, and C–H at 1438 cm^{-1}. GO contributed most to the FTIR spectra in N3, especially after the area after 1718 cm^{-1}, where the intensity of C=O at 1718 cm^{-1} and C–H at 1438 cm^{-1} significantly increased [53]. Moreover, the sign of GO peaks presented at C–O at 1236 $cm^{-1}$and C–H at 1148 cm^{-1} [54]. The elevation of the peaks increased from three to six times in N3 compared to N1.

Interestingly, H3 and N3 should shift to higher wavenumbers (blue shift) than H1 and N1. Consequently, the

Table 3 Summarized the Ns and Hs samples' density, mechanical ultrasound, velocity, compressibility, and elasticity modulus

Sample code	Density(g/mL)	Ultrasound mechanical velocity × 10^{-3} (m/s)	Compressibility × 10^{7} ($m.s^2/kg$)	Elasticity modulus × 10^{-3} ($g.m^2/mL.s^2$)
N1	0.93	33 ± 2	31.76 ± 0.22	1.05 ± 0.02
N2	1.02	44 ± 2	22.08 ± 0.12	2.02 ± 0.05
N3	**1.09**	**50** ± 3	**18.23** ± 0.10	**2.74** ± 0.04
H1	0.96	50 ± 2	20.34 ± 0.18	2.49 ± 0.05
H2	1.07	56 ± 2	17.38 ± 0.14	3.22 ± 0.06
H3	**1.12**	**65** ± 4	**13.60** ± 0.09	**4.81** ± 0.07

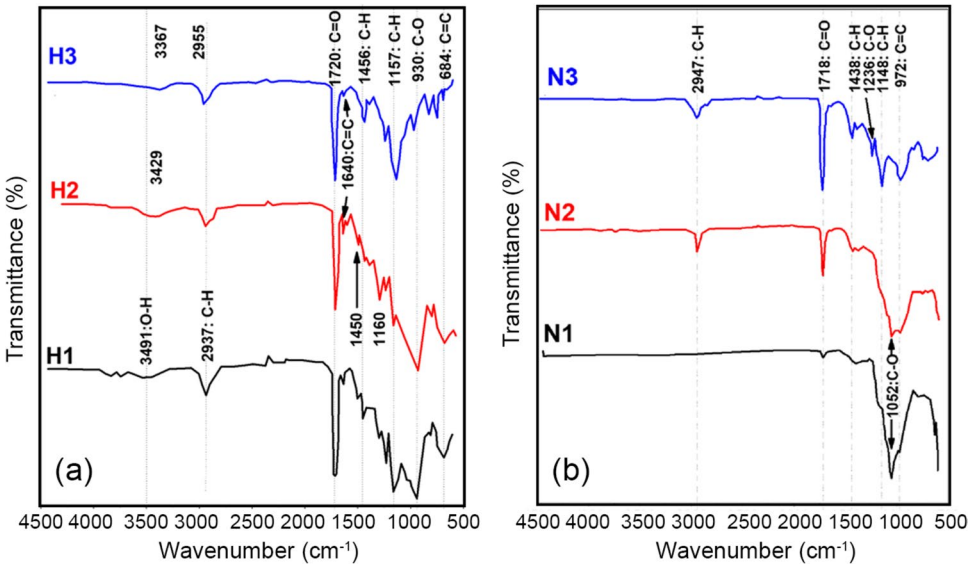

Fig. 2 FTIR spectrum for **a** hybrid samples (H1, H2, and H3), and **b** nano-samples (N1, N2, and N3) dental filling nano-composites

bond's vibrational frequency increased, signifying a rise in the bond's energy level. It signifies that the interatomic bond strength intensifies, resulting in a more inflexible link that necessitates greater energy for atomic vibrations. Consequently, vibrational frequency increases, causing the FTIR peak to move toward higher wavenumbers. Moreover, the changes in intensity peaks and presentation of the new peaks relating to the addition materials and shifting in the FTIR spectrum for both fillings referee the contribution of PMMA and GO [55], where these materials presented strong interfacial interaction and could be mainly related to hydrogen bonding presented between the components of the matrix with dental fillings [52, 56].

XRD spectra of the Hs and Ns samples are revealed in Figs. 3a and b, respectively. In Fig. 3a, H1 observed peaks at 20°, 25°, 27°, 29°, 31°, 33°, and 43°, some of these peaks are associated with the quinone of DL-camphor and Al_2O_3 as a component of Bis-GMA H filling. It matches JCPDS patterns (JCPDS 00-016-0394) of δ-Al_2O_3 and agrees with pieces of literature [57]. Interestingly, a significant change was presented after loading the PMMA in the H1, where the crystalline behavior of H2 was changed to semi-crystalline or amorphous behavior with two broad peaks between 15°

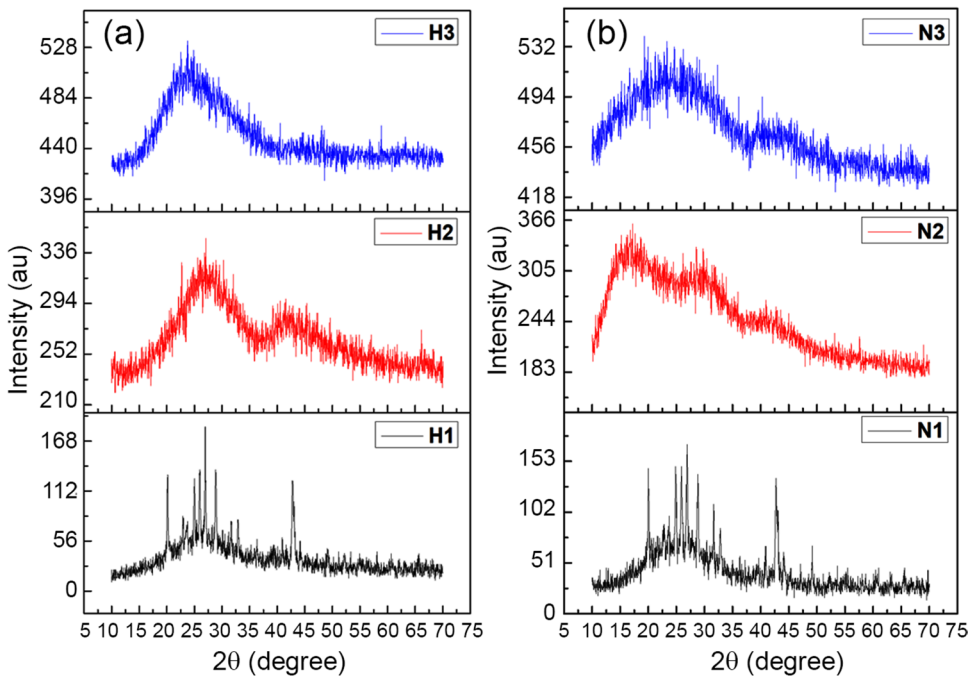

Fig. 3 XRD pattern of the **a** hybrid samples (H1, H2, and H3), and **b** nano-samples (N1, N2, and N3) dental filling nano-composites

and 35° and 35° and 50°, with the top of the peaks at 26.99°. These changes are similar to the PMMA pattern reported in the literature [58]. The incorporation of GO was associated with keeping the exact behavior of H2 by shifting the top of the first abroad peak from 26.99° to23.66°, whereas the second abroad peak disappeared.

Figure 3b displays the XRD spectra of the Ns samples. N1 observed peaks at 20°, 25°, 26°, 27°, 29°, 31.64°, 33, and 43° associated with the DL-camphor quinone [59], and Al_2O_3, which are components of the Bis-GMA in nano-filling, match the diffraction pattern (JCPDS 00–016-0394) of δ-Al_2O_3 and other findings [60]. Also, the loading of PMMA in N1 exposed a substantial change in XRD spectra to the semi-crystalline or amorphous behavior of N2 compared to the behavior of N1. N2 existed in three areas abroad with different intensities; these peaks started between 10° and 23°, 25° and 35°, and 35° to 48°. At the same time, the contribution of GO revealed two bands between 10° and 37° and 38° and 48°. N3 had two abroad peaks compared to N2, which was placed at 10°–36° and 36° to 50°. It could be related to the impact of GO and PMMA.

From Fig. 3a, the peaks of sample H2 shifted to higher values, meaning a negative strain (compressive strain) in addition to unchanging deformation of the crystal lattice as homogeneous strain (uniform strain). H3 revealed a higher intensity than H1, presenting a less homogeneous strain than H2 and H3, because of the combination of different nanomaterials in the filling. Remarkably, contributions of hybrid nanomaterials caused a small shifting in the H3 to a uniform sled to move to the positions of peak with substantial broadening. This suggests the uniform stretching or compression of the entire crystal lattice, shifting the lattice parameters across the component [61]. The revised case was presented in the Ns samples. N2 presented a small shift into lower values through the PMMA contributions associated with a uniform shift in peak positions to lower values compared with N1, with important broadening. This signifies uniformly stretched or compressed of the entire crystal lattice, shifting the lattice parameters crossways the material, whereas N3 showed a shifted peak position to advanced values. This means a negative strain (compressive strain) and uniform deformation of the crystal lattice as homogeneous strain [41] as presented in Fig. 3b.

The XRD of GO diffraction was not presented clearly in the samples, which could be related to many reasons: ratio, desperation, orientation, or overlap with other peaks due to the broad peaks given in the samples; this agrees with other investigations [62]. The XRD finding matched the FTIR results, which displayed strong interfacial interaction with the contribution of both the PMMA and GO in the matrix of both dental fillings.

The sample surface morphology is depicted using SEM images in Fig. 4 of the hybrid-filling samples. After dissolving DMF and drying as films in the experimental procedure for the SEM test, H1 displays fracture surfaces with voids and rough, gritty micro-particles. Most micro-particles were covered by loading PMMA in the H2 sample, filling the spaces and voids left by the filling matrix components. Furthermore, GO significantly influenced the fractured surface of the sample. Where H3 shows that GO is connected to creating complex links that fill in surface fractures and cracks, these links hold molecules together tightly as networks with the help of dendrimers and branches already there [52].

Figure 5 depicts the surface topography of the nano-filling sample. Figure 5 (N1) shows the composition, which consists of rough, fractured surface cavities and gritted particles, after dissolving DMF and drying as films in the experimental procedure for the SEM test. H2 exhibited surface cracks, which were associated with the PMMA surface's nature as another finding [37]. Moreover, to fill the cavities among the filling components, the morphology surface was meaningfully altered and covered the most-grained partials as revealed in Fig. 5 (N2). This remained the situation despite the filling PMMA sample filling the voids and gaps among the filling partial components. As Fig. 5 (N3) demonstrated, these fissures were sealed off, and the surface underwent significant modification by adding GO nano-sheets. The excellent contact that resulted from the constant mixing between the two components made this possible.

Long polymer chains were one of the many reasons why the morphological samples varied. It bonded the filling matrix and covered most of the particles and cavities in the dental materials. In the meantime, GO functional groups may create more significant interfacial contact between fillings, polymers, and GO as supported by FTIR spectra that clearly show this, which is consistent with a different report [63].

The TGA and DSC curves of (Hs) and (Ns) nanocomposites are revealed in Fig. 6a and b, and Fig. 7a and b, respectively. The degradation behavior of H1 showed one main segment. It degraded between 200 and 520 °C, about 17.4% at 900 °C. In contrast, the loaded PMMA showed a reduction in thermal stability and increased the degradation behavior that started earlier between 100 and 440 °C and degraded to 45.4% of H2 compared to H1 at 900 °C. Interestingly, only 10.3% of H3 was degraded at 900 °C and showed the best thermal stability with the smallest segment between 350 and 430 °C. This behavior was similar to another finding in the literature [64].

DSC characterizes the loaded material's effect on the samples' thermal transitions. As shown in Fig. 6b, H1 exhibited three glass transition temperature peaks (T_g) at 75.6, 140, and 209 °C, which related to the component of H1, while H2 showed an increase in thermal stability values of (T_g) to 85.6, 151, and 220 °C, respectively, after the addition of PMMA compared to H1. At the same time, the incorporation

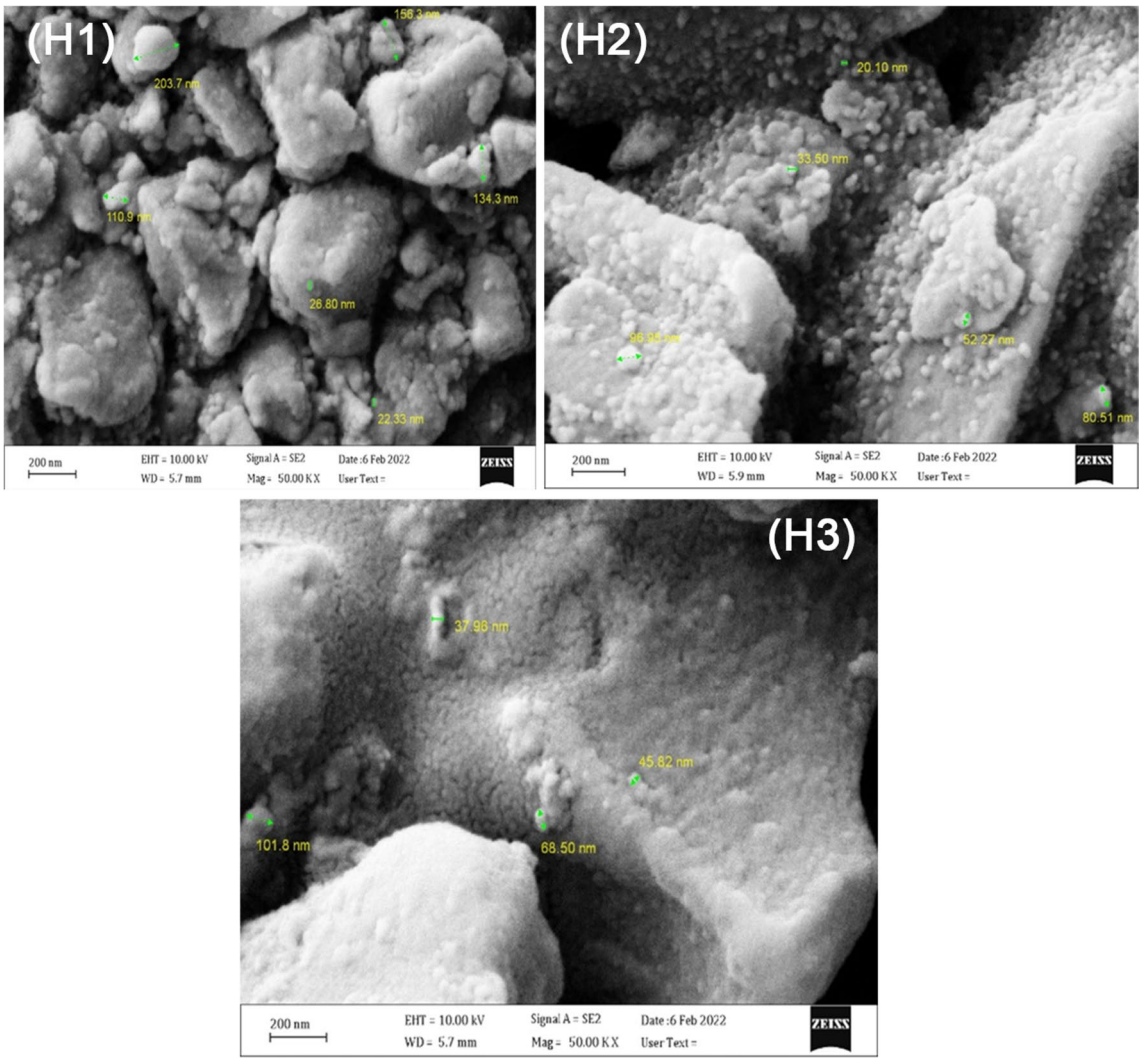

Fig. 4 SEM images of the hybrid-filling H1, H2, and H3 samples

of GO represents an increase in the (T_g) to 102, 160, and 231 °C, respectively, compared to both H1 and H2 samples.

This improvement is associated with an enhancement in the free volume and flexibility of the polymer chain with the addition of GO, which agrees with the literature [65]. The shift in peak positions to higher temperatures of T_g could be related to the interfacial interaction among filling components with GO. This interaction restricted the mobility of the chain's polymer by GO at the interface, which resulted in a reasonable improvement in structural and thermal behavior [66].

The degradation behavior of Ns samples illustrated a significant change in thermal stability after the addition of PMMA in N1, where the N1 samples also revealed one segment of degradation from 250 to 520 °C, where H1 showed 30.8% weight degradation at 900 °C. Meanwhile, N2 exhibited reduction in thermal behavior, and the degradation segment started between 170 and 435ºC. At the same time, the thermal behavior was steady until 900 °C with a degradation rate of 49.2%. Surprisingly, the GO addition improved the thermal stability by 19.7% compared to both samples. The degradation of N3 began later than other samples, between 350 and 480 °C, which was the most significant and minor degradation area for the Ns samples, as shown in Fig. 7a. Figure 7b shows the DSC of the Ns samples. N1 also exhibited three glass transition temperature peaks (T_g) at 75.5, 150, and 224 °C, while N2 exposed a slight reduction in thermal stability and values of (T_g) to 77.3, 142, and 214 °C, respectively, compared to N1. The incorporation of GO represents an increase in the (T_g) to 96.2, 156.5, and 237 °C, respectively, compared to both H1 and H2 samples

Generally, Ns were displayed, whereas PMMA revealed aim proved in thermal behavior, which is expected due to the polymer complex network formation behavior being

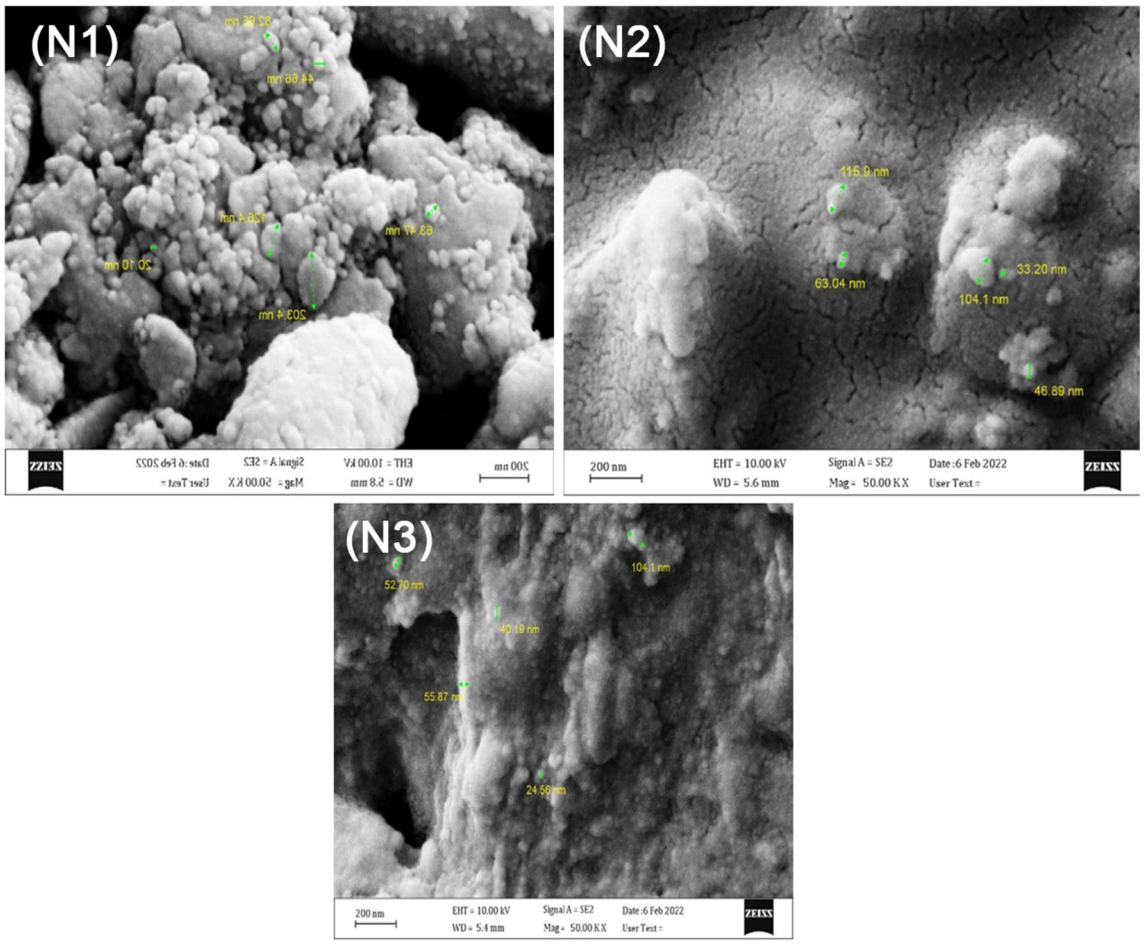

Fig. 5 SEM images of the nano-filling N1, N2, and N3 samples

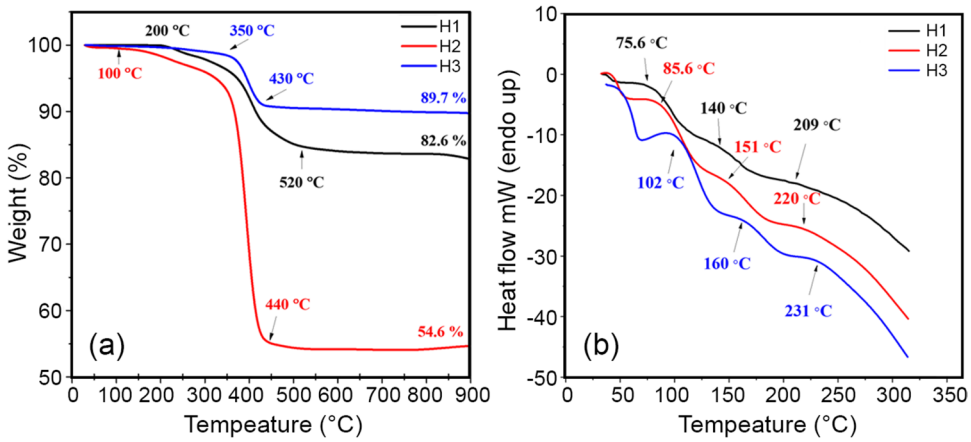

Fig. 6 **a** TGA, and **b** DSC of the hybrid-filling H1, H2, and H3 samples

higher than that of other dental materials in both groups of samples. Interestingly, the contribution of GO resulted in the restoration of Hs and Ns' dental filling, displaying better thermal behavior. In conclusion, the degradation behavior of Hs presented better thermal behavior than Ns samples before and after the contribution of GO; this behavior matches other literature findings [67].

The thermogravimetric analysis (TGA) results for Beautifil II (a giomer-based dental restorative material). Its modified versions (PMMA-filling and

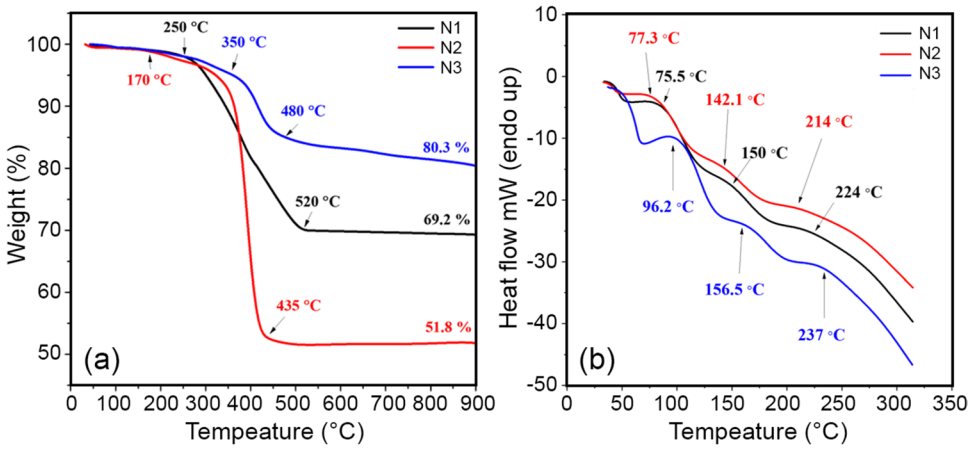

Fig. 7 **a** TGA, and **b** DSC of the N1, N2, and N3 samples

PMMA–GO-reinforced-filling) show a significant increase in residual mass, indicating improved thermal stability related to several factors of the component and composition of the materials. Where Beautifil II is a giomer (glass-ionomer + resin hybrid) containing fluoroaluminosilicate (FAS) glass fillers (inorganic, thermally stable), resin matrix (e.g., UDMA, TEGDMA) that decomposes at ~ 300–500 °C, and expected residue: ~ 54.6% (from TGA up to 800 °C), this residue primarily comes from the FAS glass fillers, which do not decompose. However, the organic resin burns off, leaving only the inorganic component [68, 69].

Whereas the effect of PMMA loading (residue increases to 82.6%), PMMA decomposes in two stages: ~ 200–300 °C: Side-chain scission (loss of ester groups) and ~ 300–400 °C: Main-chain breakdown, forming char [70]. The increase in the residue in the PMMA-filling could be related to the fact that PMMA does not fully volatilize; some carbonaceous residue remains. Moreover, adding PMMA slows the release of volatile decomposition products from the underlying resin. In addition, PMMA may form a thermally stable interface with the glass particles [71], while the effect of PMMA–GO reinforcement on the filling (residue reaches 89.7%), where GO has excellent thermal conductivity values in-plane (4000–5000 W/m.K), notably improves high thermal stability that partially reduces to thermally stable graphene-like carbon. Also, the nanosheet size of GO restricts polymer chain mobility, which delays degradation. Additionally, GO could block oxygen diffusion and volatile release [72]. Generally, GO promotes crosslinking in PMMA, increasing carbon retention, improving filler–matrix adhesion, and strengthening the PMMA–FAS glass interface due to GO's superior thermal shielding [73].

The ultrasound mechanical behavior and the related parameters of Hs and Ns samples are shown in Table 3. Density was measured from Eq. (2) using a density bottle with 25 mL, and a balance with 4-digit accuracy was utilized as presented in Table 3. The ultrasound time was substituted in Eq. (3) to calculate the ultrasound velocity, which showed an increase of 50% with loading the PMMA and GO in the H3 sample compared to H1, whereas N3 improved by 30% compared to N1. The compressibility of samples was calculated from Eq. (4), which reduced up to 74% after the incorporation of PMMA and GO compared with H1, whereas N3 improved up to 49.5% compared to N1. Elasticity modulus was calculated from Eq. (5). The results of the elasticity modulus improved after restoring the filling of H3 up to 160% compared with H1, whereas it enhanced up to 93% of N3 compared with N1. Interestingly, the Hs samples showed better ultrasound mechanical results than the Ns samples. This behavior can relate to the large volume of the polymeric chains bonded and interacting with each other [74]; in addition, the GO nanosheet from the other side increased the interfacial interaction among the dental fillings, strongly agreed with FTIR, TGA, and DSC results, and matched other findings [75].

According to the results from the structure, TGA/DSC, and ultrasound mechanical behavior, samples N3 and H3 showed the best results among their group samples N and

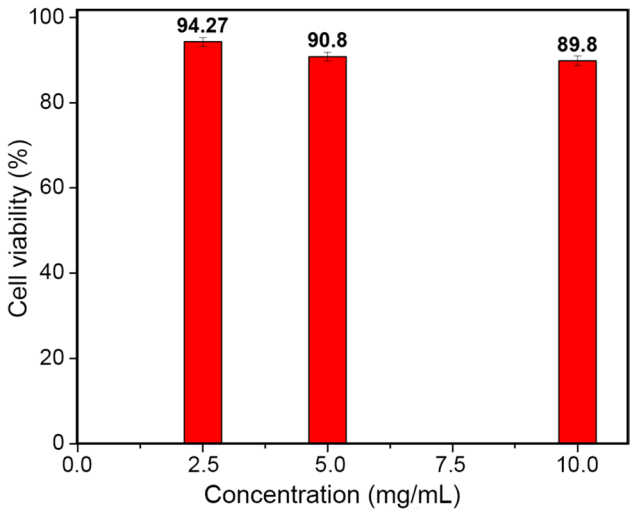

Fig. 8 Cytotoxicity with different concentrations of H3 in REF cells

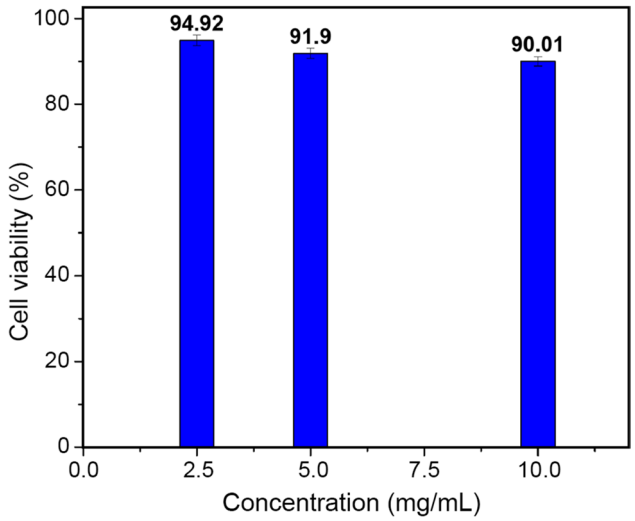

Fig. 9 Cytotoxicity with different concentrations of N3 in REF cells

H, respectively. N3 and H3 reveal the best improvement in thermal stability and mechanical behavior, with the samples being the most improved compared with the original dental filling. N3 and H3 were selected to do a cytotoxic test to ensure they are not toxic for future dental filling applications. The cytotoxic impact of X-SUBSTANCES, in contrast to REF cells, was investigated. The anti-proliferative activity of the X-SUBSTANCES was established by examining their ability to inhibit the proliferation of the REF cell line, as exposed in Figs. 8, 9, 10.

The cytotoxic effect of X-SUBSTANCES against REF cells was investigated. Cell viability revealed up to 94.27 ± 1.050%, 90.80 ± 1.069%, and 90.77 ± 1.148% of 2.5, 5, and 10 mg/mL concentration for H3, respectively. It was slightly reduced to 89.77% by increasing the concentration of the H3 from 25% to100%, which was (10 mg/mL). At the same time, cell viability revealed up to 94.92% ± 1.05%, 91.90 ± 1.156%, and 90.01 ± 1.056% of 2.5, 5 and 10 mg/mL concentrations of N3, respectively, which was slightly decreased to 90.01% with increasing the concentration from 25 to 100%, which was (10 mg/mL). Both samples revealed good cell viability results, whereas N3 revealed slightly better results than H3, which agrees with other findings [76, 77].

Conclusion

In this investigation, methods were successfully presented for the restoration of two types of dental filling by PMMA and GO. The FTIR presented a strong interaction between the component matrix and GO nanomaterials. SEM morphology images exposed the surface of the dental filling

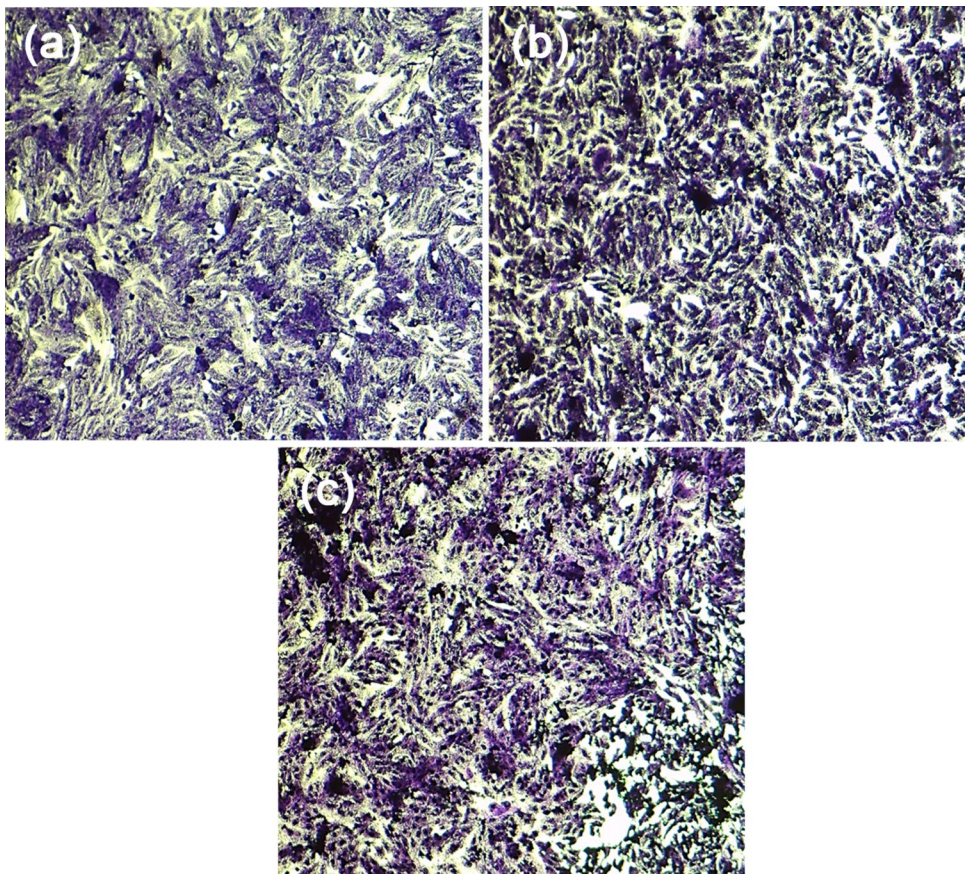

Fig. 10 Photographs with magnification of 40X for REF cells morphological changes before and after being treated with **a** control un-treated, **b** H3, and **c** N3

and almost inhibited cavities and cracks after PMMA–GO contributed. Thermal stability was impacted and improved by up to 65% of H3 with the contribution of PMMA–GO, in addition to increasing the restriction of the polymer chain and other components in the matrix of the material, which was associated with increasing the glass temperatures in the materials. Mechanical ultrasound velocity is enhanced by up to 50% of H3 compared to H1, and elasticity modulus is improved by up to 160% of H3 compared to H1. In contrast, compressibility is reduced by up to 74% of H3 compared to H1. Cell viability was present in 94.92% of restoration fillings. These results exposed the notable improvement in the thermal stability and excellent cytotoxicity of promising dental nanocomposites.

Supplementary Information The online version contains supplementary material available at https://doi.org/10.1007/s13726-025-01540-9.

Acknowledgements Abbas Kadhim Hassan would like to thank the University of Babylon, Iraq for supporting his PhD study.

Author contributions Abbas Kadhim Hassan prepared the experiment, got the results, and wrote the first draft of the submission. Habib Hamidinezhad and Ehssan Al-Bermanyare, the supervisors who designed and planned the project. Ehssan Al-Bermany synthesized the GO and did the OM and mechanical. Habib Hamidinezhad participated in the experiment's conception and improved the manuscript's quality. All authors read and approved the final manuscript.

Funding Not applicable.

Data availability The data are available in the manuscript.

Declarations

Conflict of interests Not applicable.

Ethical approval Not applicable.

Consent to participate Not applicable

Consent for publication Not applicable

References

1. Yadav R, Kumar M (2019) Dental restorative composite materials: a review. J Oral Biosci 61:78–83. https://doi.org/10.1016/j.job.2019.04.001
2. Yadav R, Singh M, Meena A (2023) Selection and ranking of dental restorative composite materials using hybrid entropy-VIKOR method: an application of MCDM technique. J Mech Behav Biomed Mater 147:106103. https://doi.org/10.1016/j.jmbbm.2023.106103
3. Yadav R (2022) Fabrication, characterization, and optimization selection of ceramic particulate reinforced dental restorative composite materials. Polym Polym Compos 30:1–10. https://doi.org/10.1177/09673911211062755
4. Saini S, Meena A, Yadav R, Patnaik A (2023) Investigation of physical, mechanical, thermal, and tribological characterization of tricalcium phosphate and zirconia particulate reinforced dental resin composite materials. Tribol Int 181:108322. https://doi.org/10.1016/j.triboint.2023.108322
5. Tuama AN, Al-Bermany E, Alnayli RS (2024) A critical review of the evaluation of SiO_2-incorporated TiO_2 nanocomposite for photocatalytic activity. SILICON 16:2323–2340. https://doi.org/10.1007/s12633-024-02870-8
6. Hashim FS, Jabbar SA, Al-Bermany E, Abdali K (2024) Effect of inclusion ZnO-Co_3O_4 nanoparticles on the microstructural and optical properties of PVA-CMC polymeric blend for biomedical, UV shielding, and nuclear radiation shielding applications. Plasmonics 20:1629–1641. https://doi.org/10.1007/s11468-024-02379-1
7. Al-Abbas SS, Ghazi RA, Al-shammari AK (2021) Influence of the polymer molecular weights on the electrical properties of poly(vinyl alcohol)-poly(ethylene glycols)/graphene oxide nanocomposites. Mater Today Proc 42:2469–2474. https://doi.org/10.1016/j.matpr.2020.12.565
8. Yadav R, Meena A (2022) Effect of aluminium oxide, titanium oxide, hydroxyapatite filled dental restorative composite materials on physico-mechanical properties. Ceram Int 48:20306–20314 https://doi.org/10.1016/j.ceramint.2022.03.311
9. Beyth N, Domb AJ, Weiss EI (2007) An in vitro quantitative antibacterial analysis of amalgam and composite resins. J Dent 35:201–206. https://doi.org/10.1016/j.jdent.2006.07.009
10. Jabbar SA, Khalil SM, Abdulridha AR (2022) Dielectric, AC conductivity and optical characterizations of (PVA-PEG) doped SrO hybrid nanocomposites. Key Eng Mater 936:83–92. https://doi.org/10.4028/p-41a757
11. Ferracane JL, Hilton TJ (2016) Polymerization stress:is it clinically meaningful? Dent Mater 32:1–10. https://doi.org/10.1016/j.dental.2015.06.020
12. Abdali K, Abass KH, Al-Bermany E (2022) Morphological, optical, electrical characterizations and anti- *escherichia coli* bacterial efficiency (AECBE) of PVA/PAAm/PEO polymer blend doped with silver NPs. Nano Biomed Eng 14:114–122. https://doi.org/10.5101/nbe.v14i2.p114-122
13. Nayak M (2020) Effect of modern (junk) food in dental caries. Indian J Forens MedToxicol 14:9194–9197
14. Cheng L, Zhang K, Weir MD et al (2015) Nanotechnology strategies for antibacterial and remineralizing composites and adhesives to tackle dental caries. Nanomedicine 10:627–641. https://doi.org/10.2217/nnm.14.191
15. Kassardjian V, Andiappan M, Creugers NHJ, Bartlett D (2020) A systematic review of interventions after restoring the occluding surfaces of anterior and posterior teeth that are affected by tooth wear with filled resin composites. J Dent 99:103388. https://doi.org/10.1016/j.jdent.2020.103388
16. Weiss EI, Enoch O, Steinkeller-Dekel M (2023) Effect of composite resin containing antibacterial filler on sugar-induced pH drop caused by whole saliva bacteria. J Prosthet Dent 130:938.e1-938.e7. https://doi.org/10.1016/j.prosdent.2023.09.015
17. Beyth N, Farah S, Domb AJ, Weiss EI (2014) Antibacterial dental resin composites. React Funct Polym 75:81–88. https://doi.org/10.1016/j.reactfunctpolym.2013.11.011
18. Salgado H, Fonseca P, Vaz M (2022) The use of graphene for dental polymethylmethacrylate reinforcement:a systematic review. Revista Portuguesa de Estomatologia, Medicina Dentaria e Cirurgia Maxilofacial 63:179–188
19. Hu W, Peng C, Luo W (2010) Graphene-based antibacterial paper. ACS Nano 4:4317–4323. https://doi.org/10.1021/nn101097v
20. Şuhani MF, Băciuţ G, Băciuţ M (2018) Current perspectives regarding the application and incorporation of silver nanoparticles into dental biomaterials. Med Pharm Rep 91:274–279
21. Imazato S, Ma S, Chen J, Xu HHK (2014) Therapeutic polymers for dental adhesives: loading resins with bio-active components.

Dent Mater 30:97–104. https://doi.org/10.1016/j.dental.2013.06.003
22. Aldulaimi NR, Al-Bermany E (2021) New fabricated UHMWPEO-PVA hybrid nanocomposites reinforced by GO nanosheets: structure and DC electrical behaviour. J Phys Conf Ser 1973:012164. https://doi.org/10.1088/1742-6596/1973/1/012164
23. Lorusso F, Inchingolo F, Greco Lucchina A (2021) Graphene-doped Poly(methyl-methacrylate) as an enhanced biopolymer for medical device and dental implant. J Biol Regul Homeost Agents 35:195–204
24. Rashid A-KJ, Jawad ED, Kadem BY (2011) A study of some mechanical properties of Iraqi palm fiber-PVA composite by ultrasonic. Eur J Sci Res 61:203–209
25. Rokaya D, Srimaneepong V, Sapkota J (2018) Polymeric materials and films in dentistry: an overview. J Adv Res 14:25–34. https://doi.org/10.1016/j.jare.2018.05.001
26. Ghazi RA, Al-Mayalee KH, Al-Bermany E (2022) Impact of polymer molecular weights and graphene nanosheets on fabricated PVA-PEG/GO nanocomposites: morphology, sorption behavior and shielding application. AIMS Mater Sci 9:584–603. https://doi.org/10.3934/matersci.2022035
27. Hassan AK, Hamidinezhad H, Al-Bermany E (2024) Antibacterial activity and optical behavior for restoration of micro and nano dental fillers using functional graphene nanosheets with polymethyl methacrylate. Nano Biomed Eng 16:652–664. https://doi.org/10.26599/NBE.2024.9290075
28. Yadav R, Meena A, Lee SY, Park SJ (2024) Experimental tribological and mechanical behavior of aluminium alloy 6061 composites incorporated ceramic particulates using Taguchi analysis. Tribol Int 192:109243. https://doi.org/10.1016/j.triboint.2023.109243
29. Yadav R, Lee H, Lee JH (2023) A comprehensive review: physical, mechanical, and tribological characterization of dental resin composite materials. Tribo Int 179:108102
30. Ahamad Said MN, Hasbullah NA, Rosdi MRH (2022) Polymerization and applications of poly(methyl methacrylate)-graphene oxide nanocomposites: a review. ACS Omega 7:47490–47503. https://doi.org/10.1021/acsomega.2c04483
31. Al-Bermany E, Chen B (2023) Effect of the functional groups of polymers on their adsorption behavior on graphene oxide nanosheets. Macromol Chem Phys 224:2300101. https://doi.org/10.1002/macp.202300101
32. Shahsavari S, Golshan Ebrahimi N (2022) Designing an antifungal smart release container based on halloysite nanoparticles loaded with thyme extract: fabrication of a long-term antifungal coating for PMMA dental material. Iran Polym J 31:1337–1346. https://doi.org/10.1007/s13726-022-01078-0
33. AL-Mamoori AY, Ibrahem SH, Al-Bermany E, (2025) Exploring the impact of $YBa_2Cu_3O_7$-x superconductor on optical properties of PS-PMMA composites: Insights into band gap and dielectric behavior. AIP Conf Proc 3169:060010. https://doi.org/10.1063/5.0254335
34. Jandt KD, Watts DC (2020) Nanotechnology in dentistry: present and future perspectives on dental nanomaterials. Dent Mater 36:1365–1378. https://doi.org/10.1016/j.dental.2020.08.006
35. Padovani GC, Feitosa VP, Sauro S (2015) Advances in dental materials through nanotechnology: facts, perspectives and toxicological aspects. Trends Biotechnol 33:621–636. https://doi.org/10.1016/j.tibtech.2015.09.005
36. Ahmed RM, Al-Bermany E (2024) Innovative hydrogel MC/GO-Fe3O4 nanocomposites: unveiling morphology and directorial behavior for optoelectronic device and antibacterial activity. Emerg Mater 25:1–4. https://doi.org/10.1007/s42247-024-00849-0
37. Radhi A, Mohamad D, Abdul Rahman FS (2021) Mechanism and factors influence of graphene-based nanomaterials antimicrobial activities and application in dentistry. J Mater Res Technol 11:1290–1307. https://doi.org/10.1016/j.jmrt.2021.01.093
38. Alawi AI, Al-Bermany E, Alnayli RS (2024) Impact of SiO_2–GO hybrid nanomaterials on opto-electronic behavior for novel glass quinary (PAAm–PVP–PVA/SiO_2–GO) hybrid nanocomposite for antibacterial activity and shielding applications. Opt Quantum Electron 56:429. https://doi.org/10.1007/s11082-023-06070-3
39. Ucpinar Durmaz B, Atılgan MG, Aytac A (2022) A comparative study of graphene oxide or chemically reduced graphene oxide filled poly(ethylene terephthalate)/poly(butylene terephthalate)/graphene nanocomposites. Iran Polym J 31:991–1002. https://doi.org/10.1007/s13726-022-01046-8
40. Abdul-Nabi RA, Al-Bermany E (2024) Performers of Si_3N_4concentrations on morphology and electrical behavior for new quinary fabrication PEO-CMC-PANI/GO@Si_3N_4nanocomposites for electronic devise and gas sensor application. SILICON 16:5583–5601. https://doi.org/10.1007/s12633-024-03092-8
41. Ahmed RM, Al-Bermany E (2024) Tuning the optical absorption and band gab of hydrogel methylcellulose loaded using hybrid Fe_3O_4@GO nanomaterials for optoelectronic and antibacterial activity. J Opt 3:1–5. https://doi.org/10.1007/s12596-024-02204-2
42. de Oliveira ÉC, da Silva BF, Schopf PF (2022) In vitro and in vivo safety profile assessment of graphene oxide decorated with different concentrations of magnetite. J Nanoparticle Res 24:1–17. https://doi.org/10.1007/s11051-022-05529-w
43. Aljelawy SS, Al-Bermany E, Abdulridha AR (2024) Performance of graphene-functionalized nano chitosan in ternary polymeric nanocomposites for physical and biological applications. J Polym Res 31:226. https://doi.org/10.1007/s10965-024-04064-7
44. Mahmood RI, Kadhim AA, Ibraheem S (2022) Biosynthesis of copper oxide nanoparticles mediated *Annona muricata* as cytotoxic and apoptosis inducer factor in breast cancer cell lines. Sci Rep 12:16165. https://doi.org/10.1038/s41598-022-20360-y
45. Jasim AJ, Sulaiman GM, Ay H (2022) Preliminary trials of the gold nanoparticles conjugated chrysin: an assessment of anti-oxidant, anti-microbial, and in vitro cytotoxic activities of a nanoformulated flavonoid. Nanotechnol Rev 11:2726–2741. https://doi.org/10.1515/ntrev-2022-0153
46. Al-Musawi S, Albukhaty S, Al-Karagoly H (2020) Dextran-coated superparamagnetic nanoparticles modified with folate for targeted drug delivery of camptothecin. Adv Nat Sci Nanosci Nanotechnol 11:045009. https://doi.org/10.1088/2043-6254/abc75b
47. Abbas ZS, Sulaiman GM, Jabir MS (2022) Galangin/β-cyclodextrin inclusion complex as a drug-delivery system for improved solubility and biocompatibility in breast cancer treatment. Molecules 27:4521. https://doi.org/10.3390/molecules27144521
48. Jabir MS, Taha AA, Sahib UI (2018) Linalool loaded on glutathione-modified gold nanoparticles: a drug delivery system for a successful antimicrobial therapy. Artif Cells Nanomed Biotechnol 46:345–355. https://doi.org/10.1080/21691401.2018.1457535
49. Britannica (2021) The Editors of Encyclopaedia. In: polymerEncyclopedia Britannica
50. Benaicha M, Jalbaud O, Hafidi Alaoui A, Burtschell Y (2015) Correlation between the mechanical behavior and the ultrasonic velocity of fiber-reinforced concrete. Constr Build Mater 101:702–709
51. Moridis GJ, McVay DA, Reddell DL, Blasingame TA (1994) Laplace transform finite difference (LTFD) numerical method for the simulation of compressible liquid flow in reservoirs. SPE Adv Technol Ser 2:122–131. https://doi.org/10.2118/22888-pa
52. kadhim MA, Al-Bermany E (2021) New fabricated PMMA-PVA/graphene oxide nanocomposites: structure, optical properties and

application. J Compos Mater 55:2793–2806. https://doi.org/10.1177/0021998321995912
53. Al-shammari AK, Al-Bermany E (2021) New fabricated (PAA-PVA/GO) and (PAAm-PVA/GO) nanocomposites: functional groups and graphene nanosheets effect on the morphology and mechanical properties. J Phys Conf Ser 1973:012165. https://doi.org/10.1088/1742-6596/1973/1/012165
54. Aljelawy SS, Al-Bermany E, Abdulridha AR (2025) Opto-electrical dielectrics and conductivity behavior of vinyl polymers reinforced with chitosan@graphene oxide nanomaterials for optoelectronic and biological activity. Eur Phys J Plus 140:94. https://doi.org/10.1140/epjp/s13360-025-06006-8
55. Kadhim MA, Al-Bermany E (2020) Enhance the electrical properties of the novel fabricated PMMA-PVA/graphene based nanocomposites. J Green Eng 10:3465–3483
56. Al-Bermany E, Chen B (2021) Preparation and characterisation of poly(ethylene glycol)-adsorbed graphene oxide nanosheets. Polym Int 70:341–351. https://doi.org/10.1002/pi.6140
57. Mohammed AA, Khodair ZT, Khadom AA (2020) Preparation and investigation of the structural properties of α-Al_2O_3 nanoparticles using the sol-gel method. Chem Data Collect 29:100531. https://doi.org/10.1016/j.cdc.2020.100531
58. Mohammed Ali AN, Ali NA, Hussein SI (2023) Nanoarchitectonics of silver/poly (methyl methacrylate) films: structure, optical characteristics, antibacterial activity, and wettability. J Inorg Organomet Polym Mater 33:694–706. https://doi.org/10.1007/s10904-022-02525-4
59. Febriantini D, Cahyana AH, Yunarti RT (2019) A microwave assisted, Fe_3O_4/Camphor-catalysed threecomponent synthesis of 2-amino-4H-chromenes and their antibacterial and antioxidant activity. IOP Conf Ser: Mater Sci Eng 2019:12036
60. Kim HN, Lee SK (2013) Effect of particle size on phase transitions in metastable alumina nanoparticles: a view from high-resolution solid-state 27Al NMR study. Am Mineral 98:1198–1210. https://doi.org/10.2138/am.2013.4364
61. Khorsand Zak A, Esmaeilzadeh J, Hashim AM (2024) X-ray peak broadening and strain-driven preferred orientations of pure and Al-doped ZnO nanoparticles prepared by a green gelatin-based sol-gel method. J Mol Struct 1303:137537. https://doi.org/10.1016/j.molstruc.2024.137537
62. Fu Y, Xiong W, Wang J (2018) Polyethylene glycol based graphene aerogel confined phase change materials with high thermal stability. J Nanosci Nanotechnol 18:3341–3347. https://doi.org/10.1166/jnn.2018.14635
63. Deshmukh K, Ahmad J, Hägg MB (2014) Fabrication and characterization of polymer blends consisting of cationic polyallylamine and anionic polyvinyl alcohol. Ionics 20:957–967. https://doi.org/10.1007/s11581-013-1062-3
64. Aldulaimi NR, Al-Bermany E (2022) Tuning the bandgap and absorption behaviour of the newly-fabricated ultrahigh molecular weight polyethylene oxide- polyvinyl alcohol/ graphene oxide hybrid nanocomposites. Polym Polym Compos 30:12196. https://doi.org/10.1177/09673911221112196
65. Aldosari M, Othman A, Alsharaeh E (2013) Synthesis and characterization of the in situ bulk polymerization of PMMA containing graphene sheets using microwave irradiation. Molecules 18:3152–3167. https://doi.org/10.3390/molecules18033152
66. Salam MA, Alsultany FH, Al-Bermany E (2024) Impact of graphene oxide nanosheets and polymethyl methacrylate on nano/hybrid-based restoration dental filler composites: ultrasound behavior and antibacterial activity. J Ultrasound 7:1–20. https://doi.org/10.1007/s40477-023-00855-8
67. Akram N, Saeed M, Usman M (2021) Influence of graphene oxide contents on mechanical behavior of polyurethane composites fabricated with different diisocyanates. Polymers 13:1–16. https://doi.org/10.3390/polym13030444
68. Canceill T, Pages P, Garnier S (2021) Thermogravimetric study of the behaviour of organic and inorganic polymers contained in four dental resin-based composites. Polym Polym Compos 29:1251–1258. https://doi.org/10.1177/0967391120967533
69. Drummond JL (2008) Degradation, fatigue, and failure of resin dental composite materials. J Dent Res 87:710–719. https://doi.org/10.1177/154405910808700802
70. Hussein MA (2017) Role of cross-linking process on the performance of PMMA. Int J Biosens Bioelectron 3:279–284
71. Dos Santos PB, da Silva Ribeiro HJ, Ferreira AC (2022) Process analysis of PMMA-based dental resins residues depolymerization: optimization of reaction time and temperature. Energies 15:91. https://doi.org/10.3390/en15010091
72. Al-shammari AK, Al-Bermany E (2022) Polymer functional group impact on the thermo-mechanical properties of polyacrylic acid, polyacrylic amide- poly (vinyl alcohol) nanocomposites reinforced by graphene oxide nanosheets. J Polym Res 29:351. https://doi.org/10.1007/s10965-022-03210-3
73. Naznin H, Mallik AK, Hossain KS (2021) Enhancement of thermal and mechanical properties of PMMA composites by incorporating mesoporous micro-silica and GO. Results Mater 11:203. https://doi.org/10.1016/j.rinma.2021.100203
74. Abdelamir AI, Al-Bermany E, Hashim FS (2020) Important factors affecting the microstructure and mechanical properties of PEG/GO-based nanographene composites fabricated applying assembly-acoustic method. AIP Conf Proc 2020:020110. https://doi.org/10.1063/5.0000175
75. Al-Jamal AN, O. KA, Abbass KH, (2023) Silver NPs reinforced the structural and mechanical properties of PVA-PAAm-PEG nanocomposites. AIP Conf Proc 2023:030005. https://doi.org/10.1063/5.0114621
76. Williams AG, Moore E, Thomas A, Johnson JA (2023) Graphene-based materials in dental applications: antibacterial, biocompatible, and bone regenerative properties. Int J Biomater 2023:3283. https://doi.org/10.1155/2023/8803283
77. Fadhl Abodood AA, Abdali K, Mousa Al-Ogaili AO (2023) Effect of molar concentration and solvent type on linear and NLO properties of aurintricarboxylic (ATA) organic dye for image sensor and optical limiter applications. Int J Nanosci 22:2350014. https://doi.org/10.1142/S0219581X2350014X
78. Hummers WS, Offeman RE (1958) Preparation of graphitic oxide. J Am Chem Soc 80:1339–1339. https://doi.org/10.1021/ja01539a017